Deep-Sea Research II 112 (2015) 18–30

Contents lists available at ScienceDirect

Deep-Sea Research II

journal homepage: www.elsevier.com/locate/dsr2

Interannual forcing mechanisms of California Current transports I: Meridional Currents

Andrew Davis *, Emanuele Di Lorenzo

School of Earth and Atmospheric Science, Georgia Institute of Technology, 311 Ferst Drive, Atlanta, GA 30332-0340, USA

ARTICLE INFO

Available online 20 February 2014

Keywords:
Eastern boundary currents
California Current
Transport processes
Currents
Wind stress curl

ABSTRACT

An ensemble of eddy-resolving ocean model hindcasts integrated from 1950 to 2008 is used to examine and quantify the interannual variability of large-scale (>200 km) alongshore equatorward flow in the California Current System (CCS). We also develop a single index of this transport in order to determine what fraction of variance is driven locally, by changes in wind stress curl, and remotely, by the arrival of coastally trapped waves of tropical origin.

In agreement with previous studies, coastally trapped waves dominate large-scale interannual CCS sea surface height variability. In contrast, we find that large-scale alongshore currents (v) are driven predominantly by local wind stress curl variability rather than coastally trapped waves. A simple wind-driven diagnostic model of the time-dependent large-scale geostrophic meridional transport captures $\sim$50% ($R=0.7$) of the total variance. The local wind-stress curl gradient that controls the largest fraction of meridional transport is not independent of the modulations in atmospheric circulation that drive the Pacific Decadal Oscillation (PDO), and a significant fraction of the monthly transport variability in the model ensembles is correlated to the PDO ($R=0.4$).

1. Introduction

The California Current System (CCS) comprises the Eastern Boundary Current (EBC) of the North Pacific Subtropical gyre. As an area of extensive coastal upwelling, it sustains yearly productivity, peaking in summer (Hickey, 1998; Marchesiello et al., 2003). Like other EBCs, it is also a vital nutrient and temperature transport pathway for lower latitudes, making it an important component of the Pacific climate system (Gruber et al., 2006). Although the large-scale seasonal and upwelling dynamics of the CCS are well understood, the drivers of interannual modulation of the mean current systems that comprise the California Current remain a subject of debate.

It has been suggested (Clarke and Dottori, 2008) that, in the CCS, interannual variability of sea surface height (SSH) and meridional velocity (v) is primarily forced remotely, by an equatorial SSH signal propagating first poleward along the coast as a coastally trapped wave (CTW) and then offshore as a long Rossby wave (Fig. 1A). This mechanism would also give rise to temperature, subsurface salinity (Dottori and Clarke, 2009), and plankton anomalies (Clarke and Dottori, 2008). The SSH signal would then generate geostrophic alongshore currents and tilt isopycnals, causing horizontal and vertical advection. This would imply a greater role for ENSO and other low-latitude phenomena in determining the physical and biological variability of the CCS. If the CCS were forced primarily by local wind anomalies, it would instead suggest that the CCS is a more closed, self-contained system. Our aim is to determine whether an equatorial signal entering the domain through CTW's (remote forcing) or local atmospheric variability (local forcing) dominates interannual variability of surface meridional currents in a realistic, eddy-resolving model of the CCS.

The CCS region is strongly stratified and has a narrow continental shelf, making it particularly conducive to the generation and propagation of CTW's. These waves have been detected by in situ measurement (Mooers and Smith, 1968) for over 40 years, and have also been established to be a driver of alongshore shelf currents (Hickey, 1984). They propagate at speeds between 40 and 90 cm/s (Enfield and Allen, 1980) and transmit coastal sea level and cross-shelf velocity signals poleward. Equatorially originating CTW's are a strong source of interannual variability that has been associated with ENSO (Hickey, 1984; Pares-Sierra and O'Brien, 1989). Although CTW's can be generated within the CCS region by wind stress curl anomalies or riverine input (Gill, 1982), our primary interest is in low-frequency CTW's of equatorial origin.

* Corresponding author.
E-mail addresses: andrew.davis@gatech.edu (A. Davis), edl@gatech.edu (E. Di Lorenzo).

http://dx.doi.org/10.1016/j.dsr2.2014.02.005
0967-0645

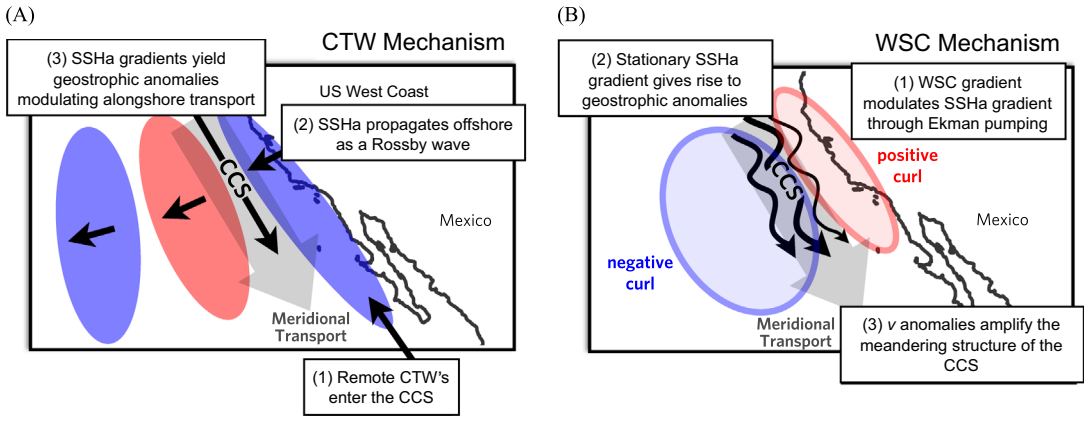

Fig. 1. Conceptual diagrams of the (A) coastal-trapped wave (CTW) and the (B) wind stress curl (WSC) mechanisms of CCS alongshore current (v) variability.

While it has been established (Enfield and Allen, 1980; Enfield and Allen, 1983; Chelton and Davis, 1982; Battisti and Hickey, 1984) by in situ measurement (largely tide gauges) that equatorially generated CTW's play a major role in the low-frequency fluctuations in SSH of the Eastern Pacific coast (within 100–200 km of shore), it remains an open question as to whether they strongly influence variability in SSH and currents further offshore (>200 km) in EBC regions.

CTW amplitude decreases exponentially away from a coastline, but the signal can travel offshore by means of a Rossby wave. For a wave of specific frequency, there exists a critical latitude Φ_c. At latitudes where the value of $\Phi<\Phi_c$, the response to an SSH anomaly is that of a CTW, whereas where $\Phi>\Phi_c$, energy propagates westward as a low-frequency Rossby wave (Schopf et al., 1981; Cane and Moore, 1981). The critical frequency for Rossby wave propagation from a purely meridional boundary at latitude Φ has been determined to be

$$\omega_c=\frac{c_1}{2tan(\phi)r_e} \tag{1}$$

where c_1 is the phase speed of the first-mode gravity wave, and r_e is the radius of the earth. Critical frequency will decrease both with increasing latitude and with any deviations from a strictly meridional coastline (due to a reduced beta effect) (Fu and Qiu, 2002). Clarke and Shi (1991) calculated the critical frequency for all of the world's major coastlines. In the CCS region, these frequencies are all on the order of around one year. Because of bottom frictional effects, as well as energy leaking as Rossby waves, CTW's will be necessarily damped as they propagate (Dorr and Grimshaw, 1986). This effect should be amplified by the geometric irregularity of the California coastline (Grimshaw and Allen, 1988). For this reason, the variance explained by coastally-originating Rossby waves can be expected to decrease poleward.

While remote forcing is transmitted by CTW's, on yearly time scales local forcing is dominated by wind stress anomalies and associated Ekman pumping (Hickey, 1998). The resulting SSH and v anomalies propagate westward as Rossby waves.

Our central question is whether low-frequency variability of meridional currents in the CCS are due to the influence of local wind stress or remote CTW-generated Rossby waves. Observations of SSH from the TOPEX/Poseidon satellite have shown that the influence of coastally generated slow Rossby waves in the Northern Pacific is limited to a region 3000–4000 km offshore. Local wind-driven waves (reconstructed from climatological data) account for nearly all of the variance in the central North Pacific, but have less influence in nearshore (<1000 km offshore) regions like the CCS (Fu and Qiu, 2002).

Recent analysis of coastal northeast Pacific ROMS hindcasts has found that while CTW's excited by equatorial sea surface height anomalies did penetrate as far as the Gulf of Alaska, variability was largely accounted for by local rather than remote forcing (Hermann et al., 2009; Masson and Fine, 2012).

Using SSH, zonal and meridional surface velocities u and v, temperature and salinity data from California Cooperative Oceanic Fisheries Investigations (CalCOFI), Dottori and Clarke (2009) concluded that dynamic height anomalies (and the associated horizontal currents and vertical motion of the thermocline) in the CCS are dominated by long Rossby waves, particularly those excited equatorially by CTW's (Fig. 1A). The spatial and temporal aliasing of the CalCOFI sampling grid may allow reasonable resolution of the SSHa transients associated with CTW/Rossby waves $\sim$100–200 km but does not resolve the effects of the meandering currents that are characterized by finer scale structure (<200 km), necessitating a modeling approach.

We propose a revised wind stress curl mechanism (Fig. 1B) dominating the low-frequency modulation of CCS meridional transport. Through Ekman pumping, wind stress curl alters the background stationary SSH gradient and generating geostrophic anomalies.

In a shallow-water quasi-geostrophic framework, wind stress is the primary driver of vorticity.

$$\frac{D(\zeta+\beta y+(f_0/H)\eta)}{Dt}=curl(\tau) \tag{2}$$

With a standard streamfunction, this can be linearized to yield

$$\frac{\partial\nabla^2\psi}{\partial t}+\beta\psi_x-\frac{1}{L_d^2}\frac{\partial\psi}{\partial t}=curl(\tau) \tag{3}$$

where L_d represents the Rossby radius of deformation. An assumption of large spatial scales leads us to neglect relative vorticity and beta terms. Differentiating in x leaves that

$$\frac{\partial v}{\partial t}=L_d^2\frac{\partial(curl(\tau))}{\partial x} \tag{4}$$

We propose that these dynamics govern the large-scale variability of CCS meridional transports and energize the regional scale meandering jets.

Our approach is to hindcast the spatial and temporal evolution of SSHa and anomalous meridional currents (v_a) over the period 1950–2008 using an eddy-resolving ocean model with two configurations that respectively include and exclude the effect of CTW's of equatorial origin. Using this model output we quantify how much of the total variance of SSHa and v_a in the CCS region can be explained by CTW's and by local wind forcing. From this analysis it can be determined where and by what margin local and

remote forcing dominate the low-frequency variability of the equatorward meridional flow in California Current.

Here we make no attempt to address the relative contributions of wind stress curl and CTW dynamics to shelf variability. While event-scale tropical CTW's can have a dramatic effect on the California coastal shelf, neither models nor AVISO satellite observations can properly resolve fine-scale coastal variance, and it is not considered here. Event-scale CTW's are also outside the scope of this study, as its primary question is the degree to which remote forcing influences interannual transport variability.

Sections 2 and 3 describe the model integrations and show verification of the speed of modeled Rossby waves. Section 4 quantifies statistically how much of the variance of sea surface height (SSH) and meridional currents are accounted for by the propagation of Rossby waves of coastal origin (CTW Hypothesis). Section 5 presents a simple statistical model that links changes in wind stress curl gradient to the dominant low-frequency fluctuations of meridional currents and transport (WSC Hypothesis). Section 6 re-examines the results of Sections 4 and 5 by hindcasting the model SSH and meridional currents with a linearized vorticity equation for Rossby waves with meridionally varying wave speed inferred from the model output. Concluding remarks and discussion are presented in Section 7.

2. The Regional Ocean Modeling System (ROMS)

This work employs two Northeast Pacific regional model hindcasts from 1958 to 2008 on a 10 km grid integrated by the Regional Ocean Modeling System (ROMS). ROMS is an eddy-permitting ocean model that solves the incompressible primitive equations. Of particular importance to this work is its use of terrain-following coordinates, which allow for more accurate bottom topography effects in coastal environments (Haidvogel et al., 2008).

At the surface are prescribed fluxes of momentum and heat derived from NCEP Reanalysis II (Kalnay et al., 1996) corrected to avoid long-term drifts in the surface temperatures and salinity as in Di Lorenzo (2003). The model domain has three open ocean boundaries with a radiation boundary condition (Marchesiello et al., 2001) to allow disturbances to propagate out of the model computational domain. Also included is a nudging to time-dependent changes at the open boundary derived from the long-term hindcast of the Ocean Model of the Earth Simulator (OFES)- a global eddy-resolving model with 10 km average resolution (Masumoto et al., 2004). The ROMS integration employing this OFES boundary condition is denoted "OBC" (Table 1). The OFES hindcast also uses NCEP surface fluxes, making it consistent with our nested ROMS computations.

The global OFES-ROMS nested approach allows for the exploration the effect of CTW's of equatorial origin in the California current. The mean SSHa record for February 1998 from this OFES hindcast over the Northeast Pacific (Fig. 2A) is dominated by anomalously high coastal SSH associated with the 1998 post-ENSO event (Bograd and Lynn, 2003). This event is also evinced in the concurrent record from the ROMS OBC hindcast across its computational domain (Fig. 2B) and in the CCS region (Fig. 2C). This indicates that the equatorial signal in the OFES hindcast successfully propagated along the eastern boundary as a CTW in the ROMS integration. We test the quality of this propagation by correlating the Niño 3.4 index (a value associated with CTW activity driven by motion of the equatorial thermocline) with SSHa records from OFES (Fig. 3A) and from our ROMS-OBC hindcast (Fig. 3B). Coastal correlations peak at .7 in the OFES record (implying that roughly 50% of variance is associated with ENSO), and peak at .6 in the ROMS-OBC run (corresponding to 40% of variance explained). To explore the sensitivity of SSH and v variability in the CCS to CTW's of equatorial origin, we integrated ROMS again using NCEP surface fluxes and the radiative boundary condition, but without nudging towards the time dependent OFES boundary conditions, effectively removing the tropical CTW signal. This run is termed "no OBC" (Table 1). Corresponding correlations between this run and Niño 3.4 (Fig. 3C) are much lower, as expected. The low values indicate that while there is weak correlation associated with the ENSO-Aleutian Low teleconnection

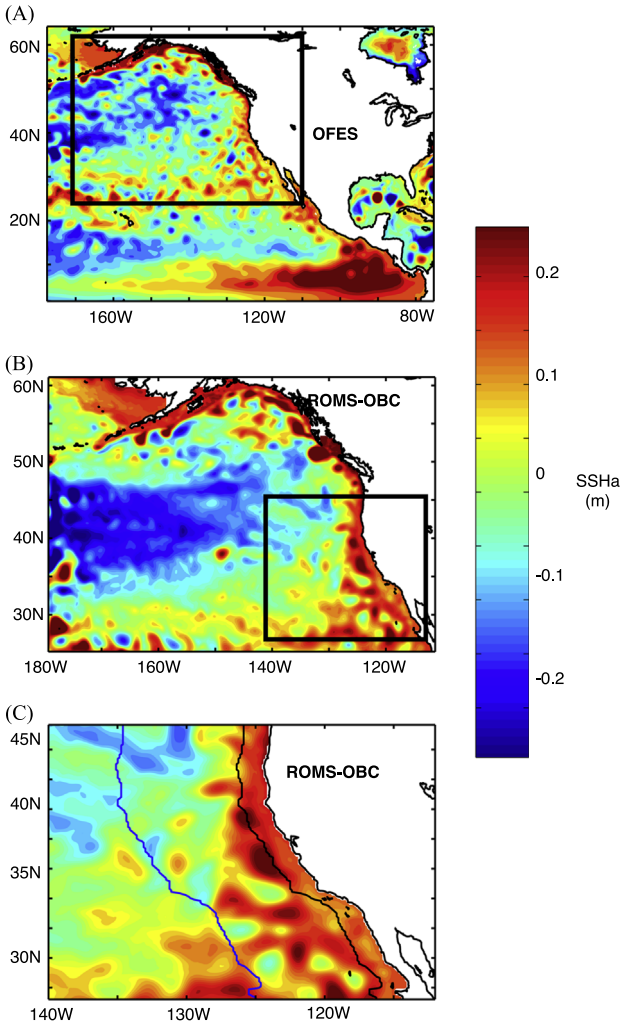

Fig. 2. (A) SSHa from the February 1998 ENSO event from the global ocean model OFES, with a black rectangle marking the computational domain of our ROMS integrations. (B) February 1998 SSHa derived from the output of our ROMS integration employing the OFES boundary condition (OBC), with a black rectangle marking the CCS region. (C) This region in more detail, with CC boundaries given by the black and blue lines. (For interpretation of the references to color in this and other figure legends, the reader is referred to the web version of this article.)

Table 1
ROMS integrations employed.

Name	Resolution	Forcing	Boundary condition	Initialization
OBC	10 km w/30 vertical levels	NCEP Reanalysis II	Radiative w/nudging to OFES	After spin-up from rest
No OBC	10 km w/30 vertical levels	NCEP Reanalysis II	Radiative w/climatology	After spin-up from rest

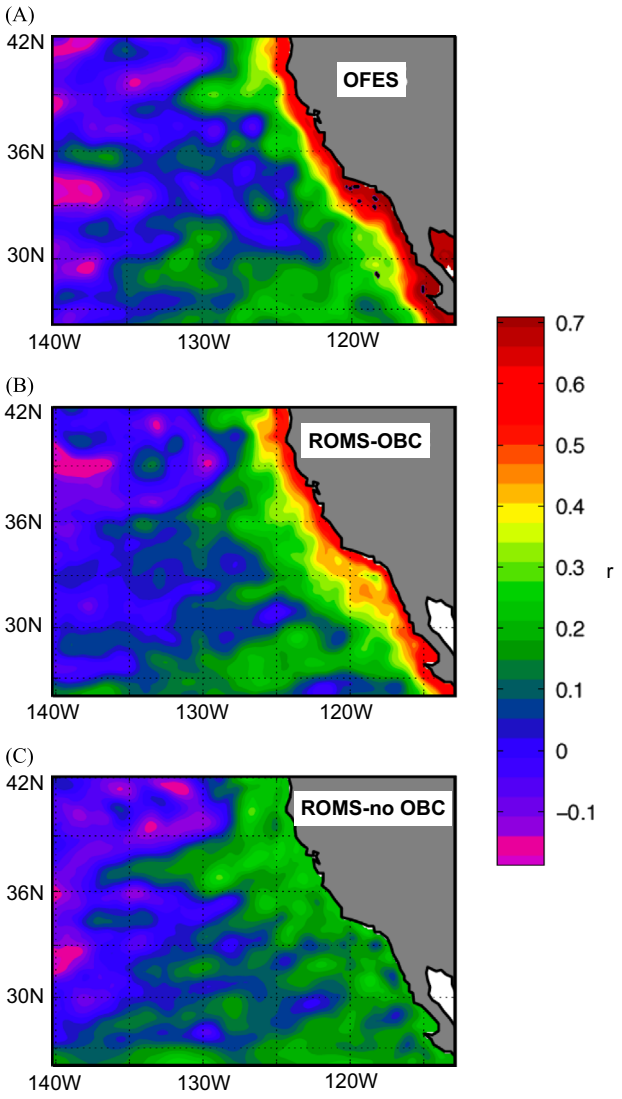

Fig. 3. (A) Correlations between Nino 3.4 and OFES SSH record, (B) SSHa from our ROMS integration using OFES boundary conditions (OBC), and (C) a ROMS integration forced only by climatology (no OBC). ROMS captures the equatorial signal, but with some damping, with a maximum correlation of 0.6 rather than 0.7 in OFES.

(Alexander, 1992), most of the SSH variance in the CCS associated with ENSO is communicated through CTW's, especially within a 100–200 km wide coastal region.

3. Speed of long Rossby waves in ROMS

Variance associated with shorter, nonlinear Rossby waves (eddies) is outside the scope of this work, so mesoscale (10–200 km) variability was removed by applying a 200 km spatial running mean to individual SSHa records. Not only does this spatial filtering remove variability associated with eddies, but it also restricts our analysis to large-scale ($>$ 200 km) Rossby waves on the order of those generated by CTW's.

To determine the phase speed of the long waves as generated by our model, we computed correlations between the SSHa time series at the coast and SSHa at all points west for lags up to 48 months for several lines of latitude – 29.1°N, 33.5°N, 37.8°N, and 41.9°N. (Fig. 4). Wave speeds calculated with this method are on the order of cm/s and decrease with higher latitude. Using these data we arrived upon an approximate set of phase speeds linearly dependent on latitude, which we used to construct SSHa and alongshore velocities in Eqs. (5) (through 9). Measured speeds went from 3.9 cm/s at 29°N (consistent with the Clarke and Dottori (2008) estimate at the latitudes of the southern CCS) to 1.9 cm/s at 42°N.

4. Testing the CTW hypothesis

In order to determine the amount of variance in SSHa associated with remote CTW forcing, we computed pointwise correlations with Niño 3.4 for lags of 0, 6, 12, and 18 months (Fig. 5A–D). The ENSO signal weakens as it propagates offshore, in agreement with theory. Corresponding maps correlating v_a and Niño 3.4 (Fig. 5E–H) show only a narrow coastal band of tropical influence which disappears at with time. A third set correlating v_a and the first time derivative of Niño 3.4 (Fig. 5I–L) (as in Dottori and Clarke's (2008) hypothesis) also shows little evidence of a remote signal.

To further study the influence of Rossby waves on SSHa and v_a, we introduce a coordinate system with the y-axis normalized to the coastline (Fig. 6A and B). We also introduce a rotated, alongshore current v_e (Fig. 6C and D). Although it captures local flow better than a purely meridional velocity, this analysis is largely insensitive to the rotation.

Using the filtering method described in Section 3, SSHa and v_e variance can be separated into large-scale and mesoscale components to establish their relative magnitudes and spatial distribution (Fig. 7). Of particular note is that large-scale SSHa variance is much stronger than the mesoscale, while the opposite is true for v_e.

To determine the fraction of variance explained by the offshore propagation of the coastal signal we computed maps of the maximum correlation between each point offshore and the coast for lags up to 3 years, as well as maps of the month in which this maximum correlation was found. These are given for the full field, the large-scale component, and the mesoscale component for both SSHa (Fig. 8) and v_e (Fig. 9). Large-scale SSHa shows a strong pattern of correlation decreasing offshore (Fig. 8B), as well as robust, linearly increasing time lags (Fig. 8D), indicating that Rossby waves play a dominant role in offshore, large-scale SSHa variance. In contrast, large-scale v_e shows strong correlations only in the nearshore (Fig. 9B). The lag at which this correlation occurs is 0 months (Fig. 9D), indicating that this is a feature of the spatial smoothing, rather than Rossby waves. This would suggest that not only is there relatively little large-scale v_e variance, but it does not propagate offshore from the coast effectively, in contrast to the CTW hypothesis. The same analysis performed on the mesoscale SSHa and v_e shows no sign of coherent offshore propagation.

5. Testing the WSC hypothesis

To determine the extent to which a stationary wind stress curl pattern drives v_e, we first computed an offshore profile of the spatially non-smoothed alongshore flow (i.e. large-scale + mesoscale) (Fig. 10A) using the normalized coordinate system shown in Fig. 6. We then computed a single time index of equatorward transport by taking a spatial mean value between 225 and 1100 km offshore, where v_e is strongly negative (e.g. the core of the CCS southward alongshore flow) (Fig. 10B). This index represents the large-scale alongshore equatorward transport associated with the CCS, but pointwise correlations between this index and v_e show (in agreement with Fig. 7F) that the velocity field is dominated by eddy-scale variance (Fig. 10C).

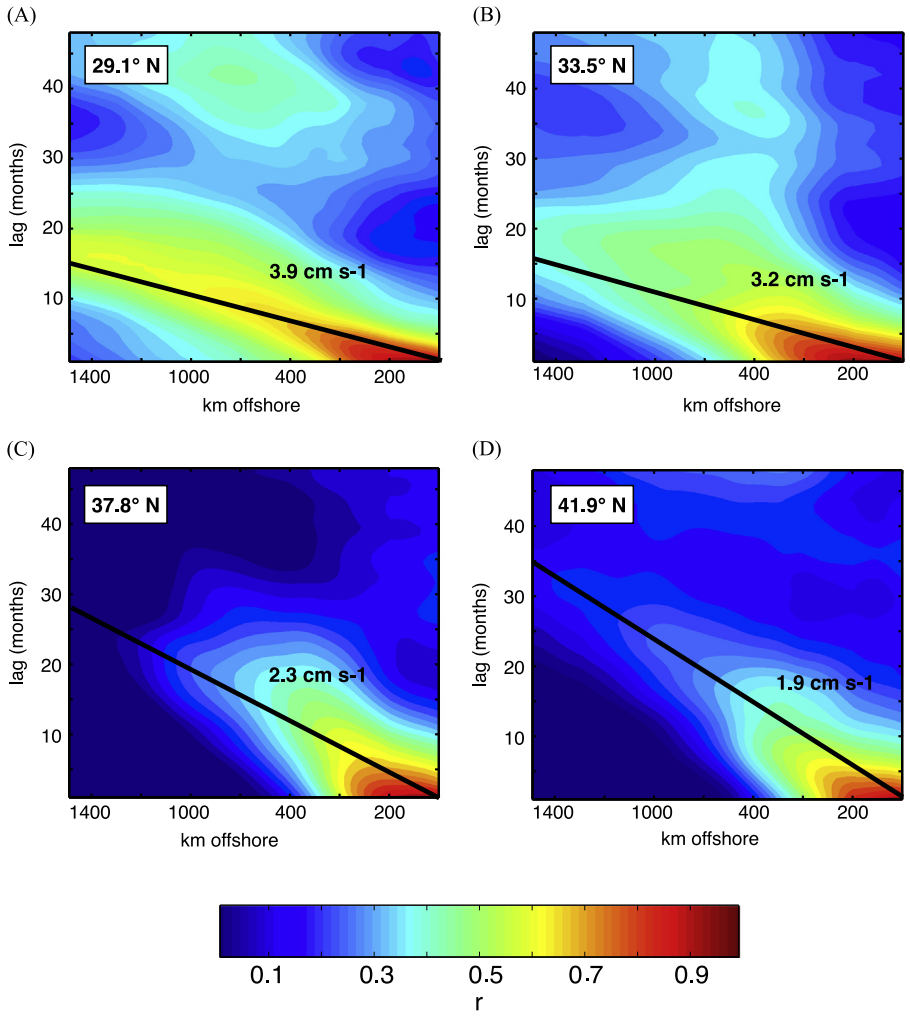

Fig. 4. Correlations between coastal SSHa and spatially filtered offshore SSHa for lags of up to 4 years by month for latitudes (A) 29.1°N, (B) 33.5°N, (C) 37.8°N, and (D) 41.9°N. The black line indicates maximum correlation and thus wave speed. Long Rossby wave speed decreases with latitude.

To determine the spatial scales that this index most effectively characterizes, we computed correlations between the index and v_e averaged zonally across the CCS region (Fig. 10C between dotted lines), and averaged meridionally in bins of varying length L_y (Fig. 10D). When L_y is less than 200 km, eddies dominate. When L_y is greater than 500 km alongshore transports become coherent. This large-scale component of transport variance is largely stationary (Fig. 9B and E), and its dynamics should follow the stationary wind stress curl balance described in Section 1. Time series of this index for the OBC and no OBC run are strongly correlated at 0.6 (not shown). The large amount of shared variance in mean v_e across both runs indicates a strong deterministic component derived from their common NCEP wind stress forcing.

Projecting the v_e index onto local NCEP wind stress curl (Fig. 11A) produces a strong large-scale cross-shelf gradient. Projecting this resulting gradient pattern onto the time dependent curl anomaly yields an index which we assume is an effective index of the wind forcing term in Eq. (4). It can accordingly be used to drive an autoregressive order-1 (AR1) model to hindcast both an index of large-scale stationary SSH gradients as well as the v_e index (Fig. 11B). The AR1 model hindcast (with a decorrelation time scale of 8 months) is strongly correlated ($R=0.7$) with the time dependent SSH index as well as the v_e index in both OBC and no OBC integrations. This confirms that the majority of deterministic large-scale meridional transport variance is driven by local wind forcing. The cross-shelf wind stress curl gradient and its associated Ekman pumping yield anomalous SSH gradients and associated large-scale geostrophic anomalies.

The pattern of wind stress curl cross-shelf gradient that drives the meridional transport (Fig. 11A) is very similar to the spatial projection of the first principal component (PC) of wind stress curl in this region (Fig. 12A), and this PC correlates with the wind stress curl gradient index at 0.9 (Fig. 12B). The similarity of the structure of the projection of this PC to the mean wind stress curl (Fig. 12C) suggests that the primary mode of wind stress curl variability (and the optimal driver of alongshore current variability) is a strengthening/damping of the stationary mean pattern. From the previous analysis we conclude that it is this dominant mode of local wind stress curl variability that forces alongshore transports in the CCS, rather than remote CTW's. This pattern of curl is not, however, fully independent of the ENSO atmospheric bridge (Alexander, 1992). During a positive ENSO phase the atmospheric teleconnections to the Aleutian Low project onto this cross-shelf pattern of the wind stress curl and drive the oceanic response of the Pacific Decadal Oscillation (PDO) in the CCS (Alexander, 1992; Mantua et al., 1997; Alexander et al., 2002). The PDO has been linked to changes in alongshore transport along the Pacific eastern boundary (Chhaak et al., 2009) and a fraction of the local CCS meridional transport variability v_e is captured by the PDO ($R=0.4$, Fig. 13).

Although these analyses suggest that Rossby waves may play only a minor role in modulating the alongshore transport in the CCS we re-examine this question using a simple Rossby wave model to

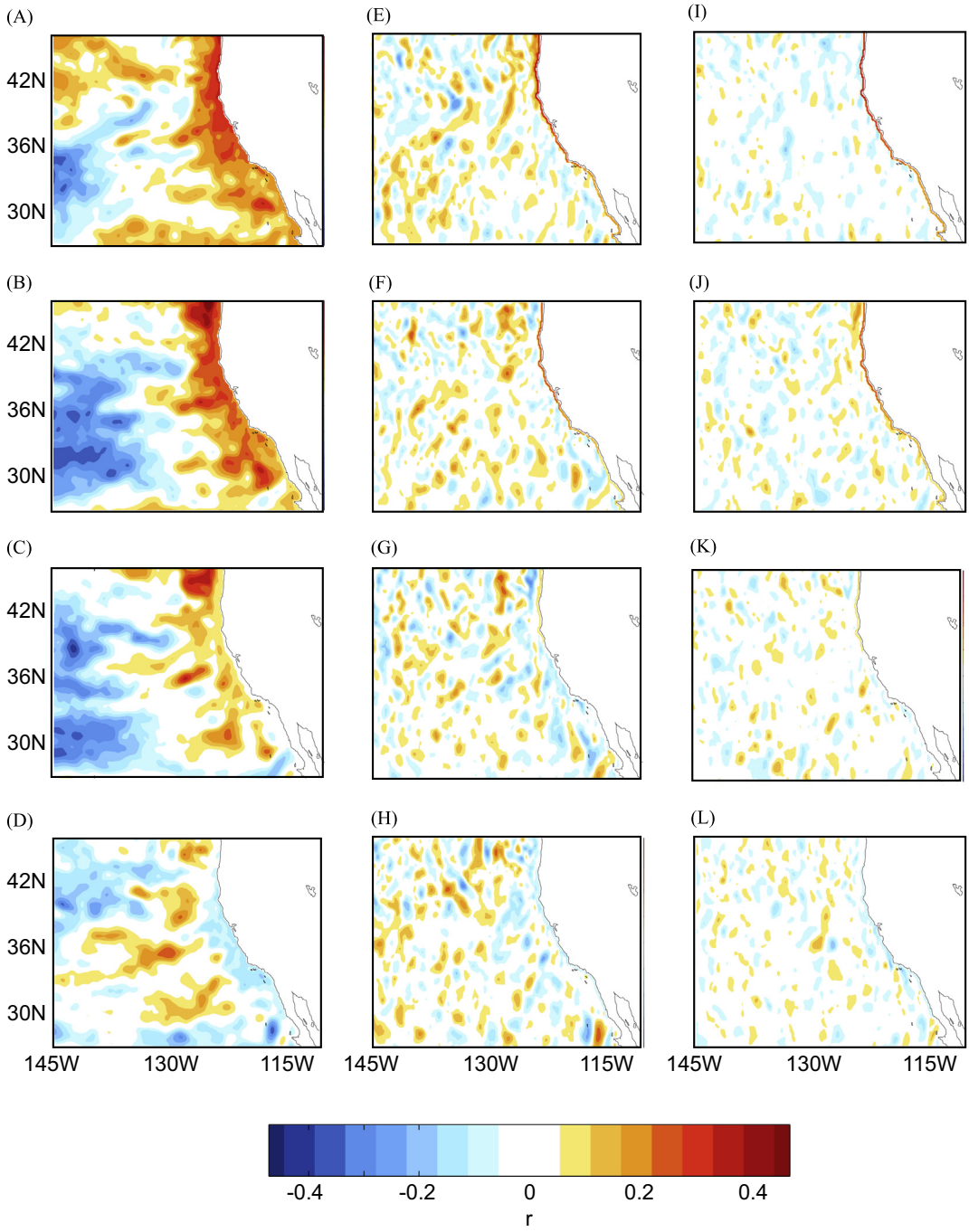

Fig. 5. Lagged pointwise correlations with Niño3.4 at 0, 6, 12, and 18 months for (A-D) SSHa and (E-H) geostrophic v_a. (I-L) Corresponding correlations between geostrophic v_a and the first time derivative of Niño3.4.

hindcast and separate the offshore SSHa and v_e variance associated with remote wave forcing and local atmospheric forcing.

6. Analytical long Rossby wave hindcast

First we used a simple forced Rossby wave model to reconstruct the large-scale sea surface height variability assuming that local winds are the primary driver of SSHa in the CCS. This hindcast employed NCEP wind stress curl records and an equation adapted from Fu and Qiu (2002),

$$h_{curl}(x,t) = k_1 \int_{x_e}^{x} \nabla \times \tau\left(x', t - \frac{x-x'}{c}\right) dx' \quad (5)$$

which integrates sea surface height h_{curl} with the curl of wind stress τ over a distance x' assuming a Rossby wave phase speed c (in a long wave approximation). k_1 is arbitrary, given that only the time variability of anomalies is relevant to the analysis. Meridional currents resulting from winds can be computed similarly assuming geostrophy (k_2 is again arbitrary).

$$v_{curl}(x,t) = k_2 \int_{x_e}^{x} \nabla \times \frac{\partial \tau}{\partial x}\left(x', t - \frac{x-x'}{c}\right) dx' \quad (6)$$

This equation can be generalized to an alongshore-oriented velocity as

$$v_{curl}(x,t) = k_2 \int_{x_e}^{x} \nabla \times \frac{\partial \tau}{\partial n}\left(x', t - \frac{x-x'}{c}\right) dx' \quad (7)$$

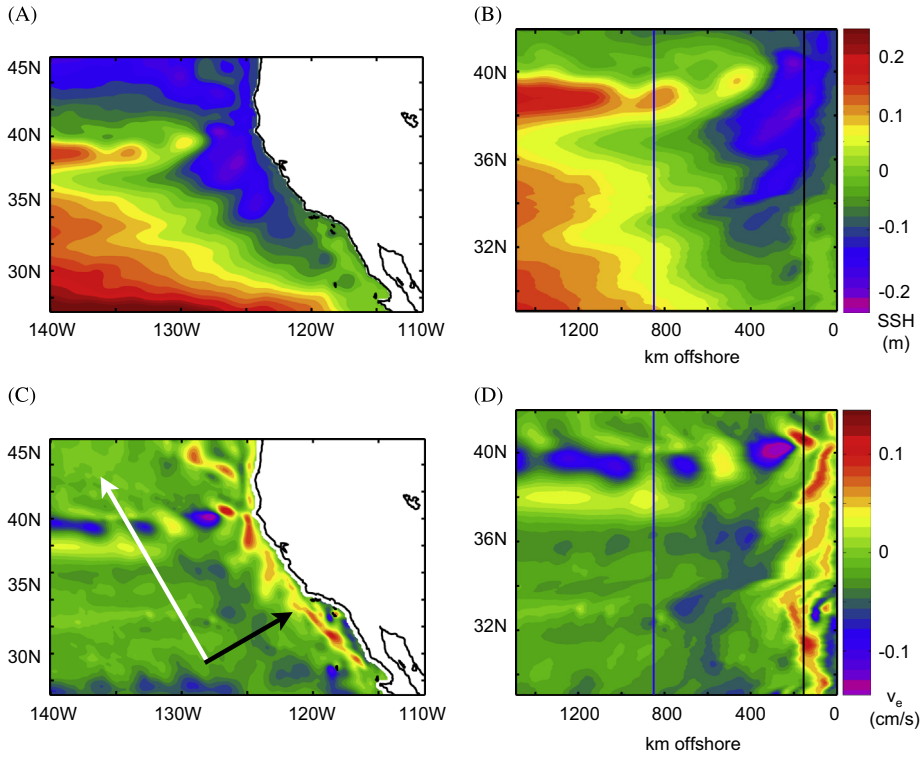

Fig. 6. (A) Mean SSH from our ROMS integration employing the OFES boundary condition, and (B) the same record in our coordinate system normalized to the coast. (C) The corresponding mean for our alongshore meridional velocity v_e. (D) The same field in the normalized coordinate system.

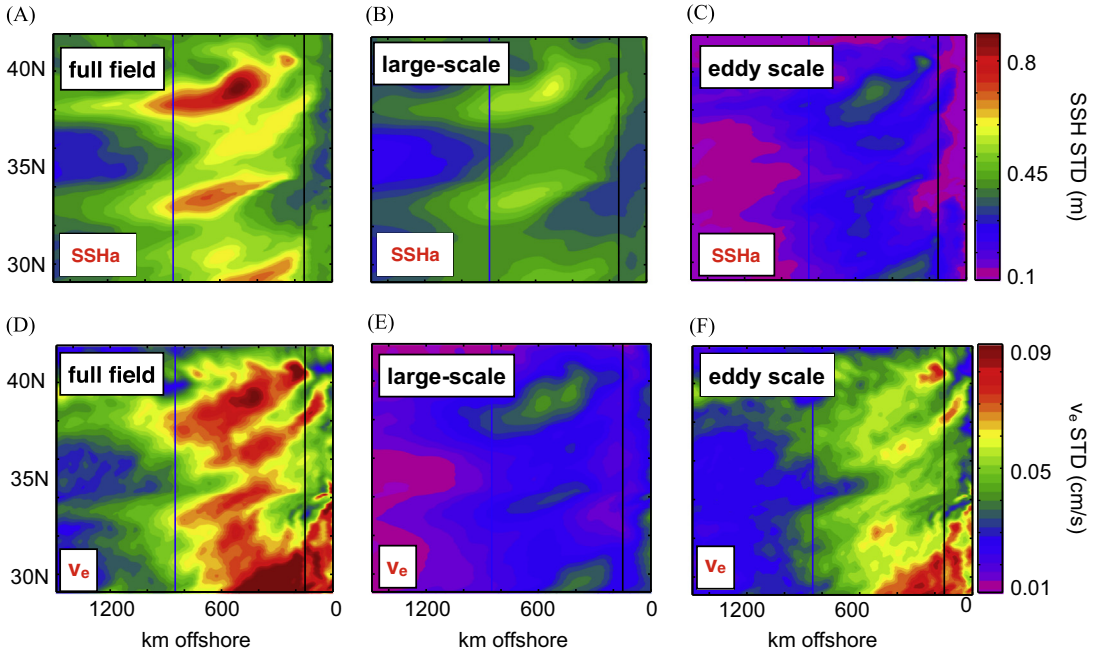

Fig. 7. (A) SSH standard deviation from our OFES boundary condition integration and corresponding plots for (B) spatial highpass (< 200 km) and (C) lowpass (> 200 km) and (D)–(F) are corresponding maps for v_e standard deviation.

where n represents a vector normal to the coast. Equivalent data sets for coastally originating Rossby waves were computed based on the assumption that on monthly time scales, variance in coastal SSH and v_e is dominated by CTW dynamics: The SSHa variability arising from Rossby waves originating from the coast (h_{coast}) is expressed as

$$h_{coast}(x,t) = h\left(x_e, t - \frac{x - x_c}{c}\right) \tag{8}$$

while the corresponding alongshore anomalies are expressed as

$$v_{coast}(x,t) = v\left(x_e, t - \frac{x - x_c}{c}\right) \tag{9}$$

We then computed correlations between these data sets and model output values for the large-scale (> 200 km) SSH and v anomalies.

Essential in constructing both of these data sets is the speed of baroclinic Rossby waves. Observed phase speeds in the ocean are

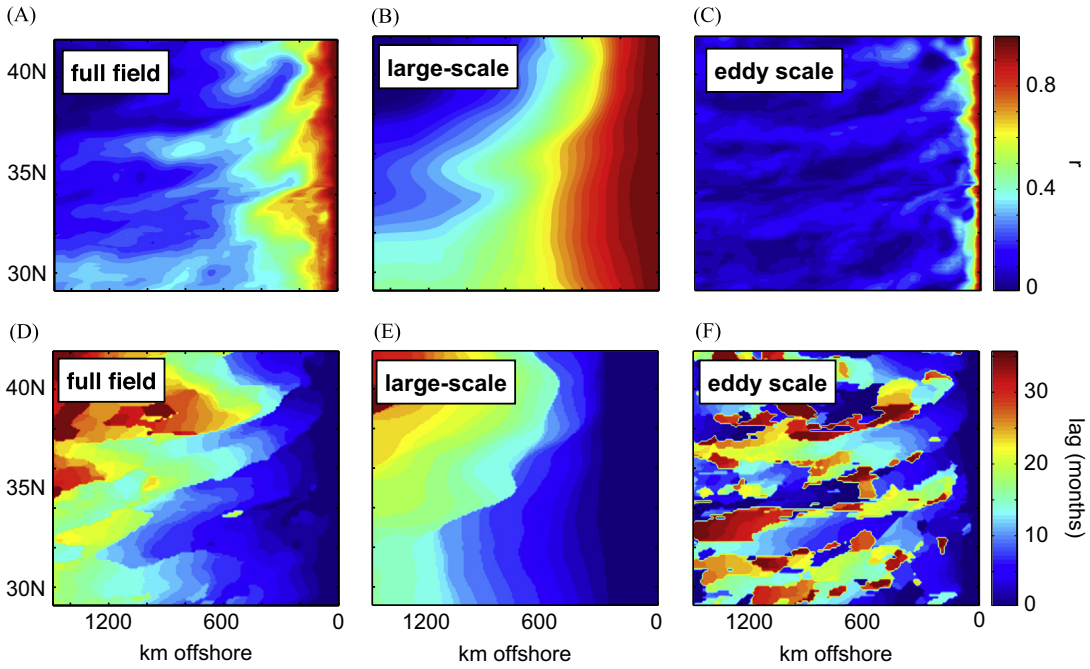

Fig. 8. (A) Maximum correlations over lags of up to 3 years between offshore and coastal SSHa using the full SSHa field, (B) the spatial-lowpassed field, and (C) the highpassed field. (D)–(F) The corresponding lags, in months, for which this maximum correlation is found.

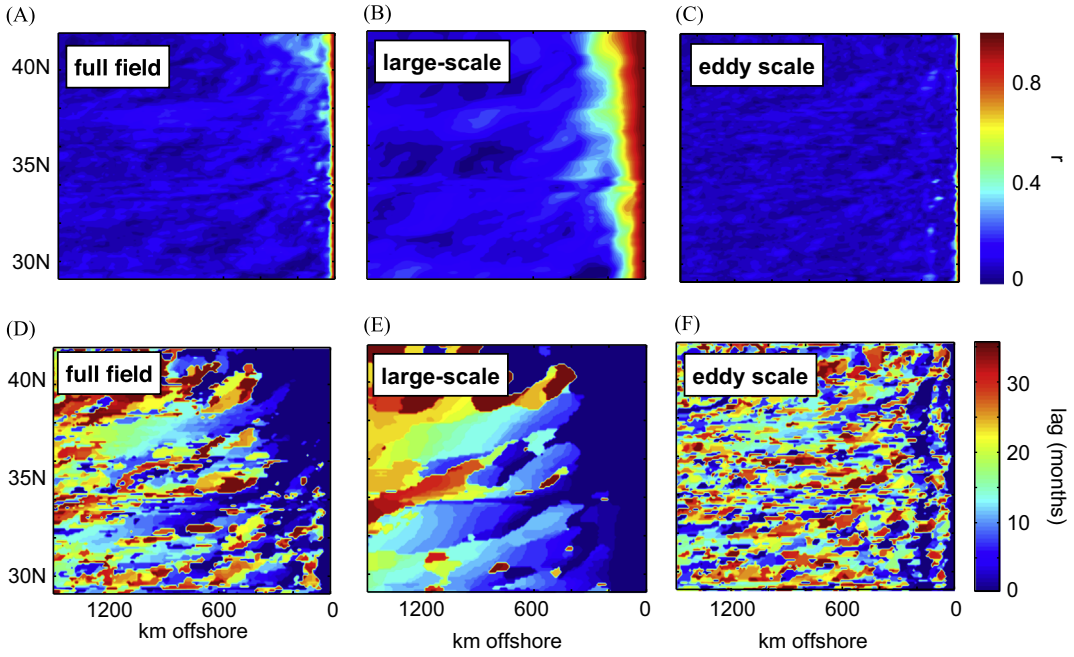

Fig. 9. (A) Maximum correlations over lags of up to 3 years between offshore and coastal v_e using the full v_e field, (B) the spatial-lowpassed field, and (C) the highpassed field. (D)–(F) The corresponding lags, in months, for which this maximum correlation is found.

between one and two times those predicted by theory, and this ratio increases with latitude. Killworth et al. (1997) argued that baroclinic zonal flows were the cause. They calculated phase speeds for the first baroclinic Rossby wave mode using observed temperature and salinity. Values for the CCS region were found to be between 1 and 3 cm/s. Dottori and Clarke (2008), however, observed dynamic height anomalies propagating through the CalCOFI sampling region at 4.1 cm/s, yet faster than a Rossby wave speed with the mean cross-shelf flow included. In our reconstructions of SSHa we used the Rossby wave speed observed in our ROMS data for a given latitude and frequency band, which vary between 3.9 and 1.9 cm/s, and are thus consistent with the Dottori and Clarke (2008) estimate.

After reconstructing synthetic data sets h_{curl} and h_{coast} using Eqs. (5) and (8), respectively, correlations were computed between large-scale SSHa and h_{curl} and SSHa and h_{coast} (Fig. 14). Variance due to wind stress curl increases at higher latitudes and in the offshore direction, and variance from CTW dynamics increases near shore and at low latitudes. The inclusion of equatorially originating CTW's (through the OBC) also increases this explained variance. It is also clear from the reconstructions that there are regions (red circles in Fig. 14A and B) where the Rossby wave model fails to capture the

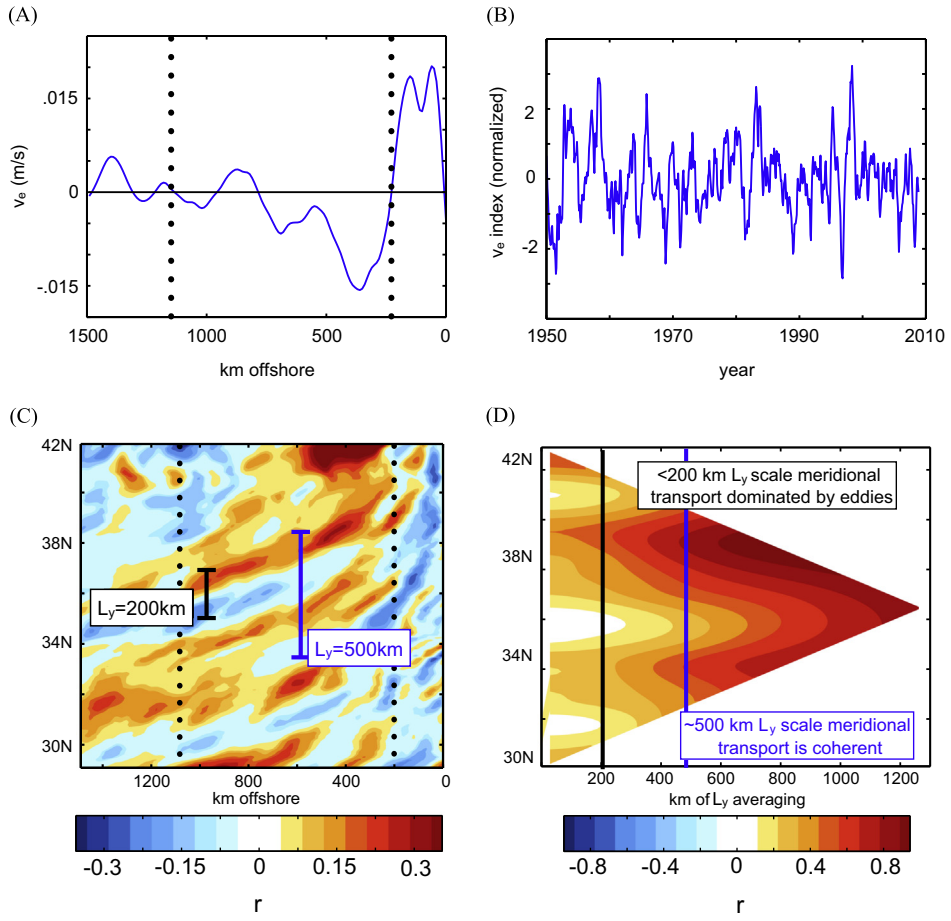

Fig. 10. (A) The offshore profile of v_e obtained from a meridional average. Dotted lines show the range over which our transport index is taken. (B) Shows this time-varying transport index. (C) Is a pointwise correlation between this index and v_e. (D) Shows the correlation between the index and v averaged into meridional bins of varying width L_y.

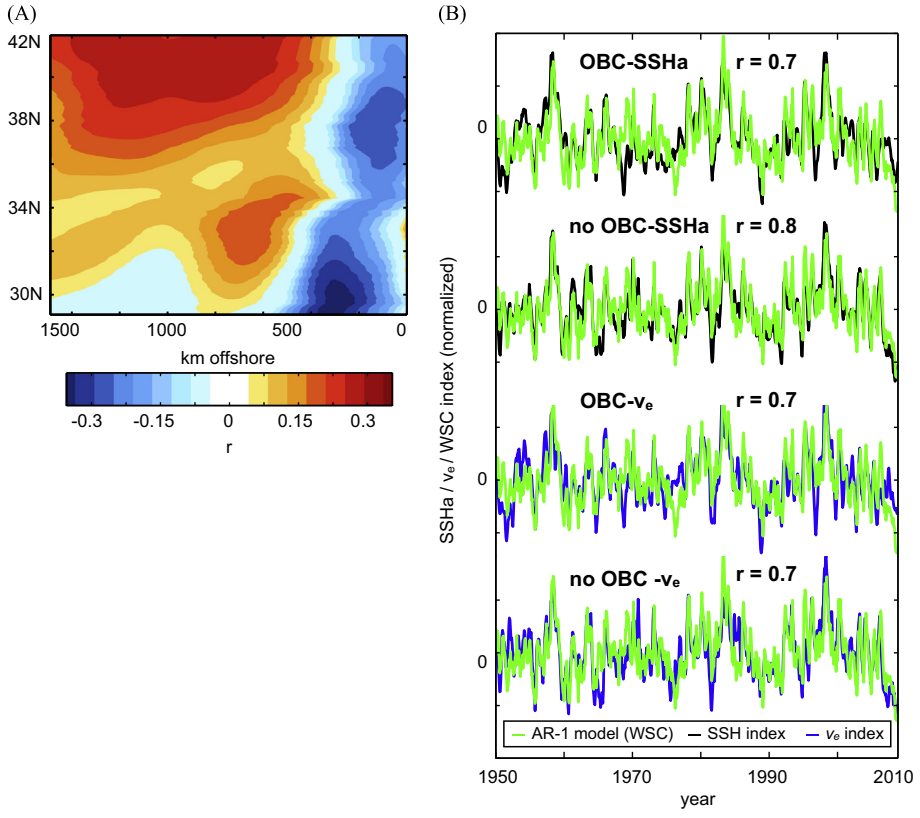

Fig. 11. (A) correlates the transport index with pointwise wind stress curl. (B) Compares a time series of an autoregressive order-1 model driven by this wind stress curl pattern with an index of the stationary large-scale cross-shelf SSH gradient, as well as the v_e transport index for both integrations.

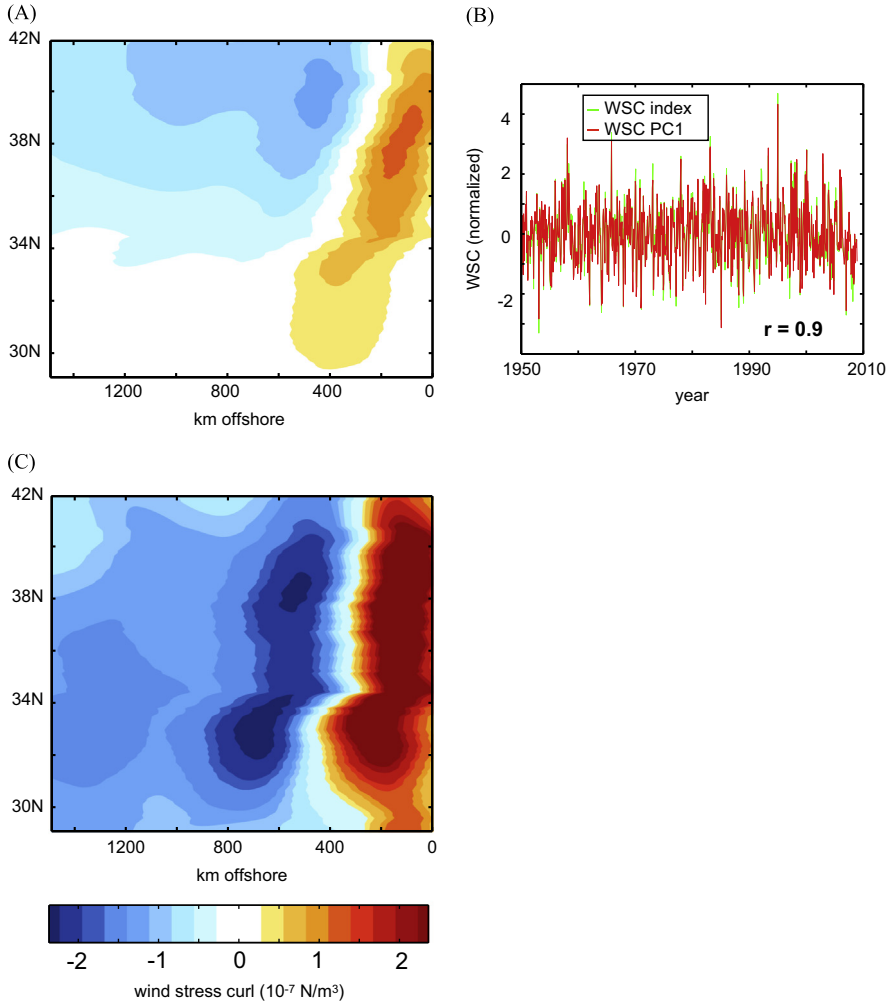

Fig. 12. (A) The projection of the first PC of CCS wind stress curl onto the full field. (B) Comparison between this PC (PC1) and the wind stress curl gradient index. (C) The local mean wind stress curl.

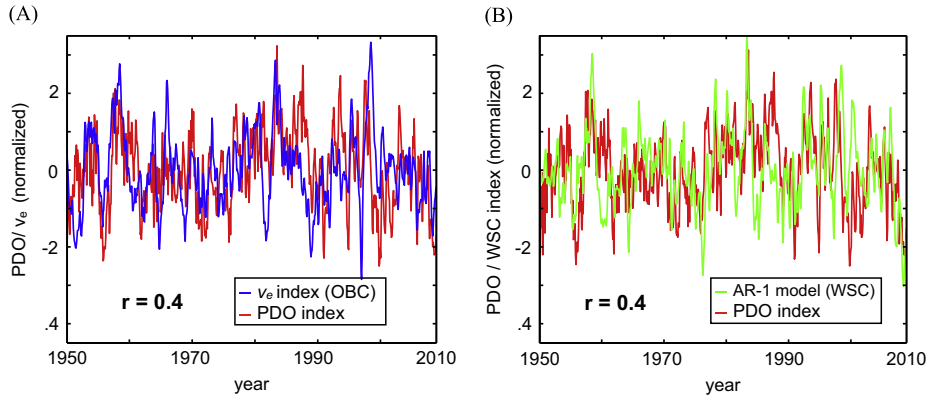

Fig. 13. (A) The PDO index compared with the v_e index (positive values indicate poleward transport). (B) The PDO index compared with the wind stress curl gradient index.

variance in SSHa. These "corridors" are located in regions where there is strong eddy shedding in the model associated with capes in the coastline (e.g. south of Pt. Conception ~34°N and off Pt. Arena ~40°N north of San Francisco).

The no OBC simulation does show a significant fraction of variance explained by coastally originating Rossby waves. This can be attributed to CTW anomalies excited within the computational domain, indicating that "semi-local" forcing also plays a role in SSH variance.

Corresponding plots were computed to determine the relative dominance of remote and local forcing in modulating v_e. First we reconstructed a v_{curl} using Eq. (6) and a v_{coast} using Eq. (8) and computed correlation maps (Fig. 15A and C). To first order, the overall hindcast skill of the Rossby wave model is significantly reduced, consistent with the findings of Section 5—that most of the meridional velocity variance is not explained by simple Rossby wave dynamics. Variance explained by CTW dynamics is further confined to a narrow nearshore region, both

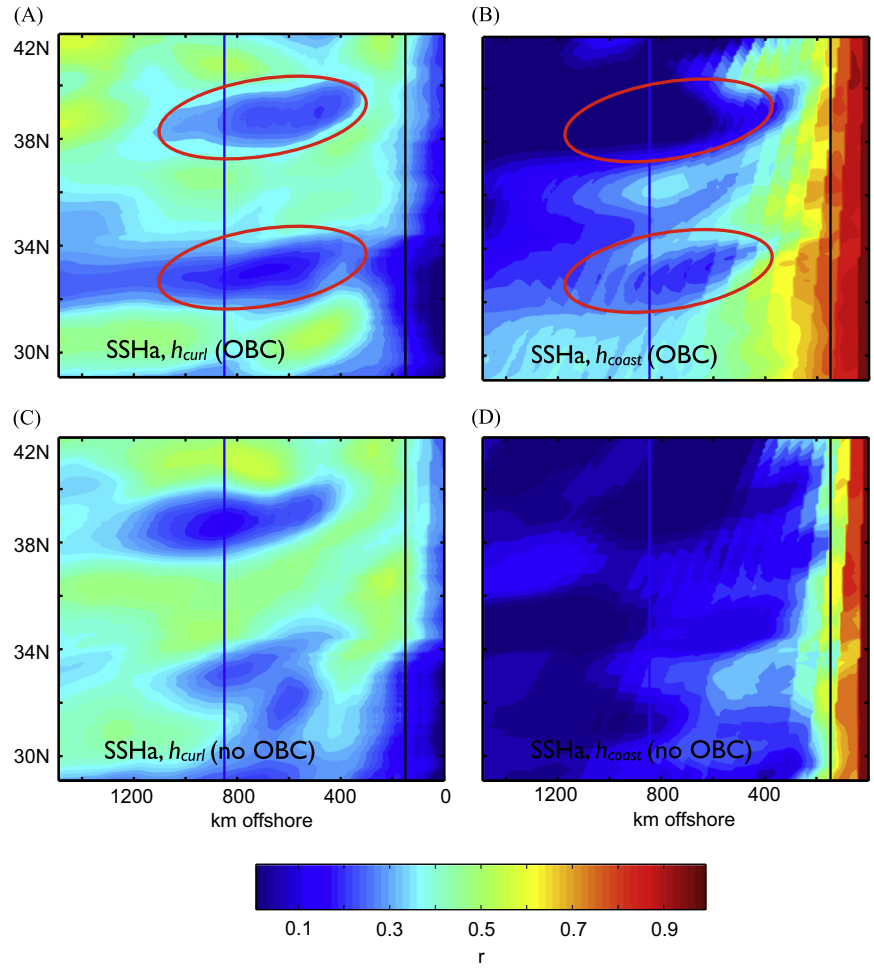

Fig. 14. (A) Correlations between SSHa derived from NCEP wind stress curl and SSHa using OFES boundary condition (OBC). (B) Correlations between Coastal SSHa and offshore SSHa using OFES boundary conditions. (C) And (D) corresponding plots for the no OBC boundary condition. All assume a Rossby wave speed that linearly decreases with latitude.

with and without the inclusion of equatorially generated CTW's (Fig. 15B and D).

7. Summary and conclusions

In this work we have explored two proposed mechanisms for the forcing of low-frequency variability of the meridional flow and transport in the California Current System. The first hypothesis maintains that mean alongshore transports are dominated by CTW variance, which radiates offshore as long Rossby waves. The associated SSHa gradients then produce anomalous geostrophic alongshore currents that control large-scale variance (Fig. 1A). The second hypothesis asserts that the local cross-shelf stationary gradient in wind stress curl anomalies alter the large-scale stationary SSH gradient through Ekman pumping (Fig. 1B).

The CTW and WSC hypotheses were tested using a set of eddy-resolving ROMS hindcasts for the period 1950–2008 that respectively included and excluded CTW's of tropical origin. Analysis of the correlation between model output SSHa and Niño 3.4 (Fig. 5A–D), as well as the effective propagation of coastal SSHa as Rossby waves (Figs. 8B,D and 14) indicated that the mechanisms of large-scale SSHa are consistent with the CTW hypothesis. However, CCS alongshore currents did not show meaningful offshore propagation (Figs. 9B,D and 15), or any tropical influence (Fig. 5E–L) and were inconsistent with this framework.

The failure of the CTW hypothesis in hindcasting CCS meridional current variability led us to explore the role of local wind forcing as the primary driver of meridional transport variability. We determined the fraction of deterministic variance associated with wind stress by developing a single index of mean alongshore transports in the two ROMS integrations with and without CTW's of tropical origin (Fig. 9). These indices track the time variability of the core of the CC equatorward flow. The correlation between the two raw monthly indices was significant ($R=0.7$) and explained a large fraction of the total variance (40–50%) indicating that most of the signal was forced locally. The role of the local forcing was further diagnosed by extracting the patterns of wind stress curl that drive the meridional transport indices. We found that a spatially stationary wind stress curl pattern with a cross-shelf gradient accounted for the largest fraction of variance in stationary SSH gradients as well as transport indices (Fig. 11B) in accordance with the dynamical theory presented in Section 1. This wind pattern is the dominant mode of local wind variability, and represents a strengthening and weakening of the mean wind stress curl cross-shelf gradient (Fig. 11).

The effectiveness of this wind stress curl pattern in hindcasting our transport index leads us to a revised system of CCS alongshore current variability. Whereas SSHa variance is concentrated on large spatial scales (>200 km), v_e is dominated by mesoscale variability (Fig. 7E and F). It is, however, energized by an offshore wind stress curl gradient, which is ultimately responsible for much of the driven large-scale (>200 km) transport variability.

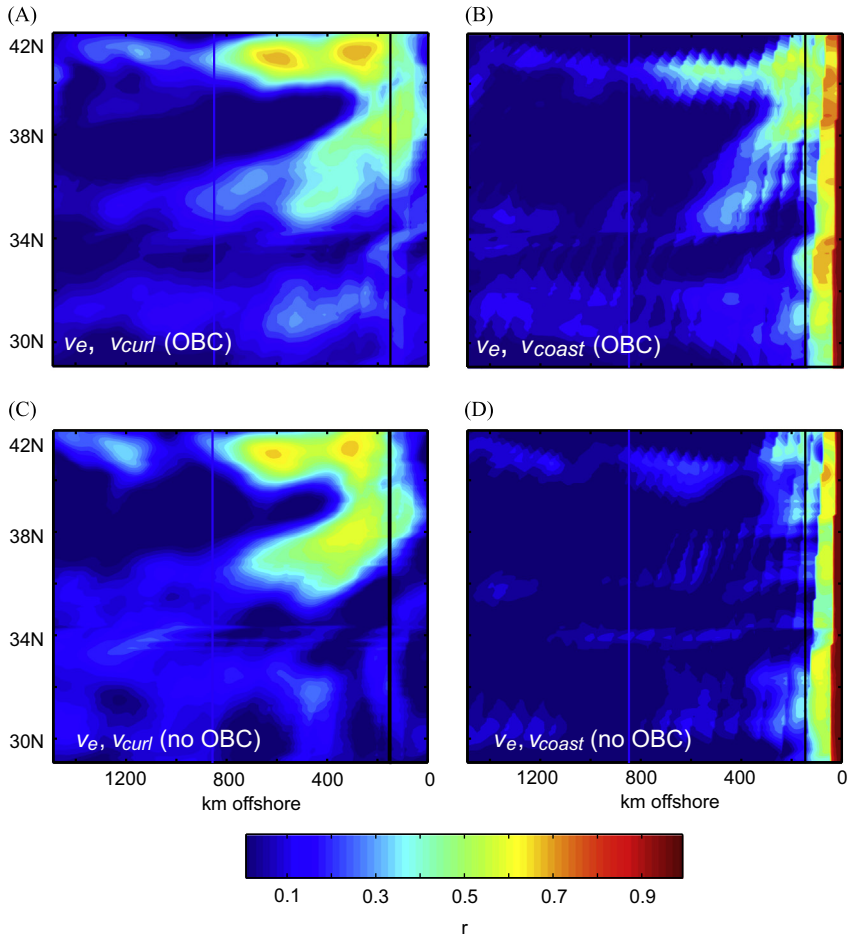

Fig. 15. (A) Correlations between v_e derived from NCEP wind stress curl and v_e using OFES boundary conditions. (B) Correlations between coastal v_e and offshore v_e using OFES boundary conditions (OBC). (C) And (D) Corresponding plots without the OFES boundary condition (no OBC).

While the CTW mechanism fails to effectively hindcast v_e, it does account for a large amount of SSHa variability. This contrast is most likely due to the large-scale Rossby waves radiated by CTW's. On monthly time scales and longer, the magnitude of velocity anomalies should be prescribed by geostrophic balance. The small wavenumber associated with these large-scale Rossby waves means that the associated gradients (and v anomalies) are small in comparison to the scale of mean flow. If we describe the SSH anomalies associated with large-scale Rossby waves as

$$SSHa = A\, e^{ik(x-ct)} \tag{10}$$

where A is an arbitrary constant, then the corresponding v anomalies will be

$$v_a = \frac{Akg}{f}\, e^{ik(x-ct)} \tag{11}$$

As the waves grow longer and k decreases, the v anomalies grow smaller as well. If, as we saw, CCS currents are best characterized by meanders and are dominated by mesoscale variance, these anomalies will have little impact on mean flow. Large-scale v anomalies are stationary, and attached to similarly stationary SSH variability. Although we made no distinction in the analysis between free tropical CTW's and semi-local wind-forced CTW's, the lack of effective propagation of transport anomalies as long Rossby waves (Fig. 9B and E) strongly suggests that neither plays a significant role in offshore flow patterns.

These results suggest a decreased role for ENSO CTW teleconnections on variability in the CCS. While ENSO SSH variability does exert control over coastal and offshore SSH signals, it has little effect on large-scale alongshore transports. This is consistent with the work of Hermann et al. (2009), Masson and Fine (2012), and Fu and Qiu (2002). Large-scale transports are forced by a specific local pattern of wind variability. However, not all the variance of the wind local forcing is independent of ENSO and the large-scale climate. The ENSO teleconnections on the Aleutian Low that drive an ocean response in the PDO pattern also project onto the local wind stress curl pattern, and a significant fraction ($R=0.4$) of meridional transport variability is captured by the PDO (Fig. 13A). This implies that low-frequency modulations of the meridional flow are also sensitive to larger Pacific climate modes through atmospheric teleconnections.

Another important observation is the small amount of variance in surface currents on long spatial scales (>200 km). We saw that large-scale v_e variance was only a small fraction of the total. This would indicate that mesoscale variance is strongly dominant in the CCS, and that interannual variations in transport are largely moderated by eddies and jets, rather than by large-scale Rossby waves. In Davis and Di Lorenzo (2015b) we examine variability on these temporal and spatial scales and find that the local wind-stress curl gradient is also an important driver of mesoscale eddies in the CCS.

References

Alexander, M.A., 1992. Midlatitude atmosphere ocean interaction during el nino.2. The Northern-hemisphere atmosphere. J. Clim. 5, 959–972.

Alexander, M.A., Blade, I., Newman, M., Lanzante, J.R., Lau, N.C., Scott, J.D., 2002. The atmospheric bridge: the influence of ENSO teleconnections on air-sea interaction over the global oceans. J. Clim. 15, 2205–2231.

Battisti, D.S., Hickey, B.M., 1984. Application of remote wind-forced coastal trapped wave theory to the Oregon and Washington coasts. J. Phys. Oceanogr. 14 (5), 887–903.
Bograd, S.J., Lynn, R.J., 2003. Long-term variability in the Southern California Current System. Deep-Sea Res. Part II—Top. Stud. Oceanogr. 50, 2355–2370.
Cane, M.A., Moore, D.W., 1981. A note on low-frequency equatorial basin modes. J. Phys. Oceanogr. 11, 1578–1584.
Chelton, D.B., Davis, R.E., 1982. Monthly mean sea-level variability along the west coast of North America. J. Phys. Oceanogr. 12, 757–784.
Chhaak, K.C., Di Lorenzo, E., Schneider, N., Cummins, P.F., 2009. Forcing of low-frequency ocean variability in the Northeast Pacific. J. Clim. 22, 1255–1276.
Clarke, A.J., Dottori, M., 2008. Planetary wave propagation off California and its effect on Zooplankton. J. Phys. Oceanogr. 38, 702–714.
Clarke, A.J., Shi, C., 1991. Critical frequencies at ocean boundaries. J. Geophys. Res.-Oceans 96, 10731–10738.
Davis, A.M., Di Lorenzo, E., 2015b. Interannual forcing mechanisms of California Current transports II: mesoscale eddies. Deep-Sea Res. Part II CCE-LTER 112, 31–41.
Di Lorenzo, E., 2003. Seasonal dynamics of the surface circulation in the Southern California Current System. Deep-Sea Res. Part II-Top. Stud. Oceanogr. 50, 2371–2388.
Dorr, A., Grimshaw, R., 1986. Barotropic continental-shelf waves on a beta-plane. J. Phys. Oceanogr. 16, 1345–1358.
Dottori, M., Clarke, A.J., 2009. Rossby waves and the interannual and interdecadal variability of temperature and salinity off California. J. Phys. Oceanogr. 39, 2543–2561.
Enfield, D.B., Allen, J.S., 1980. On the structure and dynamics of monthly mean sea-level anomalies along the pacific coast of North and South America. J. Phys. Oceanogr. 10, 557–578.
Enfield, D.B., Allen, J.S., 1983. The generation and propagation of sea-level variability along the Pacific coast of Mexico. J. Phys. Oceanogr. 13, 1012–1033.
Fu, L.L., Qiu, B., 2002. Low-frequency variability of the North Pacific Ocean: the roles of boundary- and wind-driven baroclinic Rossby waves. J. Geophys. Res.-Oceans 107, 3220, http://dx.doi.org/10.1029/2001jc001131.
Gill, A.E., 1982. Atmosphere–Ocean Dynamics. Academic Press, New York p. 662
Grimshaw, R., Allen, J.S., 1988. Low-frequency baroclinic waves off coastal boundaries. J. Phys. Oceanogr. 18, 1124–1143.
Gruber, N., Frenzel, H., Doney, S.C., Marchesiello, P., McWilliams, J.C., Moisan, J.R., Oram, J.J., Plattner, G.K., Stolzenbach, K.D., 2006. Eddy-resolving simulation of plankton ecosystem dynamics in the California Current System. Deep-Sea Res. Part I-Oceanogr. Res. Pap. 53, 1483–1516.
Haidvogel, D.B., et al., 2008. Ocean forecasting in terrain-following coordinates: formulation and skill assessment of the Regional Ocean Modeling System. J. Comput. Phys. 227, 3595–3624.
Hermann, A.J., Curchitser, E.N., Haidvogel, D.B., Dobbins, E.L., 2009. A comparison of remote vs. local influence of El Nino on the coastal circulation of the northeast Pacific. Deep-Sea Res. Part II-Top. Stud. Oceanogr. 56, 2427–2443.
Hickey, B.M., 1984. The fluctuating longshore pressure-gradient on the Pacific Northwest shelf – a dynamical analysis. J. Phys. Oceanogr. 14, 276–293.
Hickey, B.M., 1998. Coastal oceanography of Western North America from the tip of Baja California to Vancouver Island. In: Robinson, A.R., Brink, K.H. (Eds.), The Sea. John Wiley & Sons, New York, pp. 345–391.
Kalnay, E., et al., 1996. The NCEP/NCAR 40-year reanalysis project. Bull. Am. Meteorol. Soc. 77, 437–471.
Killworth, P.D., Chelton, D.B., DeSzoeke, R.A., 1997. The speed of observed and theoretical long extratropical planetary waves. J. Phys. Oceanogr. 27, 1946–1966.
Mantua, N.J., Hare, S.R., Zhang, Y., Wallace, J.M., Francis, R.C., 1997. A Pacific interdecadal climate oscillation with impacts on salmon production. Bull. Am. Meteorol. Soc. 78, 1069–1079.
Marchesiello, P., McWilliams, J.C., Shchepetkin, A., 2001. Open boundary conditions for long-term integration of regional oceanic models. Ocean Model. 3, 1–20.
Marchesiello, P., McWilliams, J.C., Shchepetkin, A., 2003. Equilibrium structure and dynamics of the California Current System. J. Phys. Oceanogr. 33, 753–783.
Masson, D., Fine, I., 2012. Modeling seasonal to interannual ocean variability of coastal British Columbia. J. Geophys. Res.-Oceans 117, 10.1029/2012JC008151.
Masumoto, Y., et al., 2004. A fifty-year eddy-resolving simulation of the World Ocean—preliminary outcomes of OFES (OGCM for the Earth Simulator). J. Earth Simul. 1, 35–36.
Mooers, C.N.K., Smith, R.L., 1968. Continental shelf waves off Oregon. J. Geophys. Res. 73, 549–557.
Pares-Sierra, A., O'Brien, J.J., 1989. The seasonal and interannual variability of the California Current System - a numerical model. J. Geophys. Res.-Oceans 94, 3159–3180.
Schopf, P.S., Anderson, D.L.T., Smith, R., 1981. Beta dispersion of low-frequency Rossby Waves. Dyn. Atmos. Oceans 5, 187–214.